RSC Advances

PAPER

View Article Online
View Journal | View Issue

Cite this: *RSC Adv.*, 2019, **9**, 12085

Solvatochromism and pH effect on the emission of a triphenylimidazole-phenylacrylonitrile derivative: experimental and DFT studies†

Karnambaram Anandhan,[a] Margarita Cerón,[a] Venkatesan Perumal,[a] Paulina Ceballos,[a] Paola Gordillo-Guerra,[a] Enrique Pérez-Gutiérrez,[a] Armando E. Castillo,[a] Subbiah Thamotharan[b] and M. Judith Percino*[a]

In this work, a study of the photophysical properties in different solvents and at different pH values of a luminogenic compound with a donor–π–acceptor (D–π–A) structure was carried out. The compound (*Z*)-3-(4-(4,5-diphenyl-1*H*-imidazol-2-yl)phenyl)-2-phenylacrylonitrile (**2**) was synthesized and characterized by SCXRD, FT-IR, ^{1}H NMR, ^{13}C NMR, EIMS, UV-Vis absorption and fluorescence. The SCXRD characterization reveals a monoclinic system, $P2_1/c$, with $Z = 4$ and an imidazole core having hydrogen bonding with respect to water molecules present in the asymmetric unit. It leads to a strong π–π-interaction in the solid state. The fluorescence λ_{max} emission of the powder and thin film was observed at 563 nm and 540 nm respectively. Several degrees of positive solvatochromic fluorescence were observed due to different molecular conformations in various solvents. When the pH of the compound was changed with HCl or NaOH, a shift in the wavelength of emission was observed in a reversible manner. At pH 2, the λ_{max} of emission was at 541 nm whereas at pH 14 there were two emissions at 561 nm and 671 nm. Due to their good emission in the solid state, compound **2** was tested as an emitting layer in OLEDs; the devices showed an acceptable performance with a luminance average of 450 cd m^{-2}. The band gap was analyzed by optical absorption, cyclic voltammetry measurement and DFT calculations.

Received 19th February 2019
Accepted 9th April 2019

DOI: 10.1039/c9ra01275c

rsc.li/rsc-advances

1. Introduction

In recent years, the π-conjugated luminophores have been extensively investigated as fluorescent sensors,[1–5] for biological imaging,[6] and for other optoelectronic applications[7–10] due to their optical properties, charge transport properties and structure tunability.[11–14] Most of the organic luminophore molecules have limitation in the fluorophore's applications, because of a strong π–π stacking interaction in the extended π-conjugated systems and dipole–dipole interaction that resulted in a weak emission or absolute absence in the condensed phase.[15,16] Also, some fluorescent compounds change their absorption wavelength and intensity of emission upon various polarity environments, *i.e.* solvatochromism phenomenon. This behaviour has attracted considerable attention because of the charge transfer nature (intra/inter molecular); it could be used as sensors of solvent polarity as well as volatile organic compounds.[17,18]

Among heteroaromatic compounds, the imidazole scaffold exhibits electron attracting or mild donating nature which displayed unique optical, thermal, electronic and biological properties.[19] Especially, 2,4,5-triphenyl-1*H*-imidazole, (lophine, Scheme 1), exhibited fluorescence and chemiluminescence properties when reacted with oxygen in the presence of strong basic conditions.[20–23] It has three phenyl groups in the C-2, C-4 and C-5 positions on the imidazole structure. Functionalized lophine derivatives are promising candidates for the light emitting applications, because it is possible to alter the structure (π-conjugation) through the phenyl ring with different donor (D) and acceptor (A). Triphenyl imidazole derivatives as well as 1*H*-imidazol-5-yl-vinyl-benz[*e*]indolium, and metal based imidazole complex showed halochromism and a discrete colour change (λ_{abs} 360, 430 and 477 nm in acidic, neutral and basic conditions respectively) on pH variation in the range of 2 to 11 and also can act as fluorescent pH sensor.[24–28] However, there are only a few optical pH sensors for use at high or low pH.[29,30]

[a]*Unidad de Polímeros y Electrónica Orgánica, ICUAP, Benemérita Universidad Autónoma de Puebla, Val 3-Ecocampus Valsequillo, Independencia O2 Sur 50, San Pedro Zacachimalpa, Pue., Mexico 72960. E-mail: judith.percino@correo.buap.mx*

[b]*Biomolecular Crystallography Laboratory, Department of Bioinformatics, School of Chemical and Biotechnology, SASTRA Deemed University, Thanjavur 613 401, India*

† Electronic supplementary information (ESI) available. CCDC 1888014. For ESI and crystallographic data in CIF or other electronic format see DOI: 10.1039/c9ra01275c

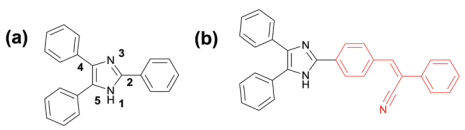

Scheme 1 (a) Numbering of the 2,4,5-triphenyl-1*H*-imidazole, (b) imidazole fused with α-cyanostilbene.

By means of pH variations, it is possible to delineate the effect of donor (push) or electron-withdrawing (pull) groups attached to C-2 of imidazole ring that decides by the electronic density of structure as well as donor capacity of N atom.

The electronic factor of the cyano group played an excellent acceptor for such D–π–A fluorescent materials which was responsible for the optical properties.[31–33] In the past decade, α-cyanostilbene derivatives have drawn attention because of their unique charge-transfer characteristics and their utility as promising fluorescent materials for use in biological, the AIE/AIEE-activity,[33] optical applications[34] and multi-stimuli responsive properties.[35–37] Our group are working to explore the photophysical and optoelectronic properties of the phenylacrylonitrile/pyridylacrylonitrile containing derivative. Based on our previously reported the strong electron withdrawing feature of the phenylacrylonitrile/pyridylacrylonitrile based chromophore that act as a good acceptor and to show an enhancement of emission in the solid state but some case its weak.[38–40] Hence it exhibited an important effect on the optical and electronic properties.[41–43]

Herein we report the synthesis of a novel imidazole derivatives containing the phenylacrylonitrile (half of the α-cyanostilbene) unit using a simple route. Even though imidazole unit has electron withdrawing nature when it combined through to the phenylacrylonitrile to examine the emission properties in the solution and solid state whether it shows enhanced or quenching. In order to find the electron charge distribution in the molecular structure (D–π–A or A′–π–A structure motif) by explore absorption and emission with varying the pH (acidic or basic conditions) and different solvents. So, the title compound undergoes a deep study of their photophysical properties in solution and solid state besides solvatochromic property, pH studies, electrochemical analysis, DFT calculations were carried out. In addition, it was evaluated as an emitting layer in OLEDs.

2. Result and discussion

2.1 Synthesis and characterisation

We reported the design and synthesis of a novel compound (*Z*)-3-(4-(4,5-diphenyl-1*H*-imidazol-2-yl)phenyl)-2-phenylacrylonitrile (**2**) as shown in Scheme 2. The 4-(4,5-diphenyl-1*H*-imidazol-2-yl) benzaldehyde (**1**) was synthesized *via* condensation of benzil with 4-formyl benzaldehyde in the presence of NH_4OAc and acetic acid at reflux for 5 hours. The compound **1** was reacted with phenyl acetonitrile with KOH as catalyst and MeOH as solvent at reflux conditions to get the compound **2** with 65% yield (Scheme 2). The principal signals in IR, ^{1}H NMR and EI for compounds **1** and **2** are summarized in experimental section.

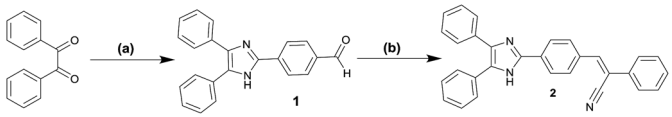

Scheme 2 Synthesis of compound **2** (a) NH_4OAc/HOAc/4-formyl benzaldehyde, reflux; (b) cat. KOH/MeOH, phenylacetonitrile, reflux.

2.2 Single crystal X-ray crystallography

Compound **2** crystallizes in the monoclinic space group $P2_1/c$ with $Z = 4$. The crystal data and refinement parameters are summarized in Table S1.† Fig. 1 shows the ORTEP diagram of the asymmetric unit of crystal **2**. The molecular structure shows the bond lengths and bond distances are also listed in Table 1. The bond distance of C(15)–N(2) is shorter, meanwhile the C(7)–N(1) and C(8)–N(2) distances are longer compared with the reported double bond lengths.[44] In addition to that, the bond C(7)–C(8) is longer and displays the electron delocalization over the atoms of C(8), C(7), N(1), C(15) of the imidazole ring. The nitrile –C(24)≡N(3) bond length is the longest N–C bond and falls into the range of a triple bond –C≡N reported for TCNQ.[44]

In the imidazole ring, the torsion angles [N(1)–C(7)–C(8)–N(2); N(2)–C(15)–N(1)–C(7); C(8)–C(7)–N(1)C(15); N(1)–C(15)–N(2)–C(8) and C(7)–C(8)–N(2)–C(15)] are smaller, indicating that the ring is found to be planar. The substituents such as phenyl groups and [2,3-diphenylprop-2-enenitrile] moiety are rotated with respect to imidazole ring, that was expected due to steric effect with dihedral angles between atoms C(5)–C(6)–C(7)–N(1) of −41.3(3)° and C(1)–C(6)–C(7)–C(8) of −40.2(3)°, whereas between [2,3-diphenylprop-2-enenitrile] attached to imidazole group is a peri-planar conformation as evident from the dihedral angles of N(2)–C(15)–C(16)–C(21) of 21.8(3)°, N(1)–C(15)–C(16)–C(17) of 22.3(3)° and the atoms C(18)–C(19)–C(22)–C(23) of −25.6(3)°; C(19)–C(22)–C(23)–C(24) of −9.3(3)° and C(22)–C(23)–C(25)–C(30) of −21.3(3)° (selected dihedral angles, bond length, bond angle and torsion angles values are in the Tables S2 to S5 in the ESI†).

The most interesting feature in the structure of compound **2** is concerned with the presence of two molecules of water in the asymmetric unit. The intermolecular motif formed by N–H···O and O(2) H···O(1) interactions are shown in Fig. 2 with hydrogen bonds distances and chain motifs a, b, c and e, and the atoms involved in chain motif formation. The water molecules in the lattice, act as H-bond donor which bridges between molecules extending along the *c* axis.

Table 2 provides a list of graph-set motif of hydrogen bonds in the compound **2** and it can be seen the –C≡N group [C(24)–N(3)] is found anti in the formed dimer. The face-to-face arrangement in Fig. 3, owing to the intermolecular interaction of O–H(solvent)···N hydrogen bond. Two neighbouring molecules stacked face-to-face manner with centroid–centroid

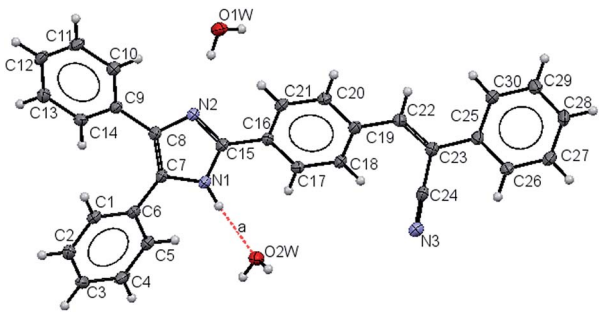

Fig. 1 ORTEP X-ray crystal structure of compound **2** and 50% of thermal ellipsoids.

Table 1 Selected bond lengths for compound 2 with reported value

Bond	Length[54] (Å)	Compound 2	Length (Å)
Imidazole			
C(sp^2)–N	1.349	C(15)–N(1)	1.349(2)
C4–N3	1.376	C(15)–N(2)	1.329(2)
C5–N1	1.370	C(7)–N(1)	1.383(2)
		C(8)–N(2)	1.380(2)
Csp^2=Csp^2	1.339	C(7)–C(8)	1.391(2)
(C=C–CAr)		C(22)–C(23)	1.358(2)
Csp^2–CAr	1.455, overall 1.460	C(8)–C(9)	1.475(2)
(conjugated)		C(6)–C(7)	1.469(3)
Csp^2–CAr C=C–CAr	1.470, overall 1.480	C(15)–C(16)	1.468(2)
(conjugated)		C(19)–C(22)	1.456(3)
		C(20)–C(21)	1.385(3)
CAr≈CAr	1.380	C(17)–C(18)	1.379(3)
C≈C (overall)	1.384	C(9)–C(10)	1.398(3)
		C(25)–C(30)	1.398(3)
Csp≡N	1.136	C(24)–N(3)	1.149(3)

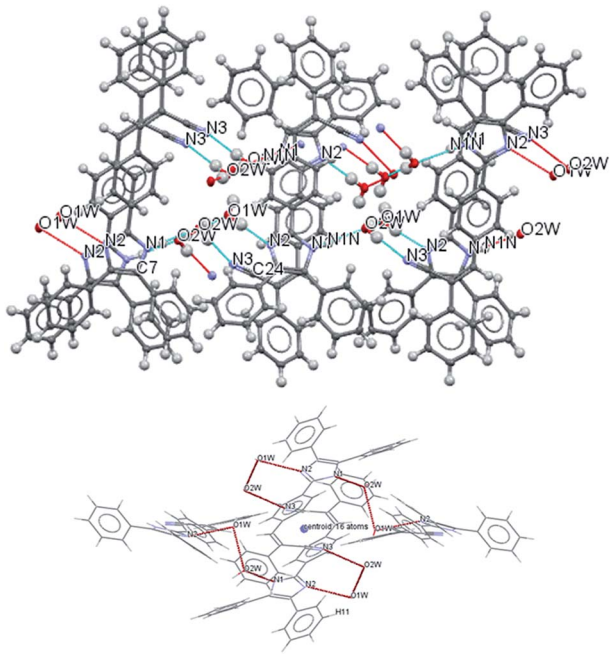

Fig. 2 Intermolecular hydrogen bond interactions between the lattice solvent molecules and compound 2.

between phenyl ring distances of 3.07 Å and off-set distance of 1.05 Å which is much shorter than reported values 1.6 – 1.8 Å (ref. 45) and this shortening causes distribution of electronic density that minimizes the π-electrons repulsion.

Fig. 4 shows the distances calculated using OLEX 246 and the typical values for aromatic π⋯π interactions (*i.e.*, the centroid–centroid distances > 3.65 Å and offsets of 1.6–1.8 Å).[45] The presence of solvent molecules in the crystal packing of compound 2 might indicate that crystal growth is optimized with O–H(solvent)⋯N(compound). The packing of structure 2 showed that the hydrogen bond interactions, the position of the nitrogen atom within the imidazole core, and the phenyl-, acrylonitrile groups play important roles and they interact with the solvent[47,48] (Fig. 4).

2.3 Optical properties

The absorption properties of compound 2 were measured in various solvents to evaluate; methanol (a protic solvent), 1,4-dioxane, $CHCl_3$, ethylacetate (EtOAc), tetrahydrofuran (THF) as well as dichloromethane (DCM), dimethylformamide (DMF),

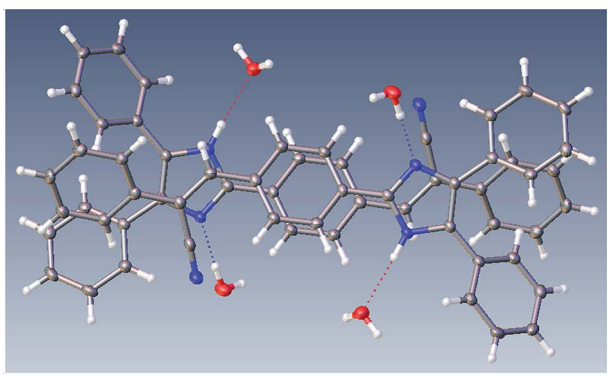

Fig. 3 Perspective view of the structures showing the strong π⋯π interactions of compound 2.

Table 2 Hydrogen-bonds D⋯H⋯A (Å) and D–HA angles (°) of compound 2

D–H⋯A		*d*(A–H)	*d*(D⋯A)	<DHA	Symmetry equivalent
O2W⋯O1W	O2W–H2(W2)	0.86(2)	2.761	174.76	$x, 1/2 - y, 1/2 + z$
N2⋯O1W	O1W–H1(W1)	0.86(2)	2.842	173.70	x, y, z
N1⋯O2W	N1–N1N	0.88(18)	2.971	170.81	x, y, z
N3⋯O2W	O2W–H2(W2)	0.84(2)	2.936	171.83	$1 - x, -1/2 + y, 1/2 - z$

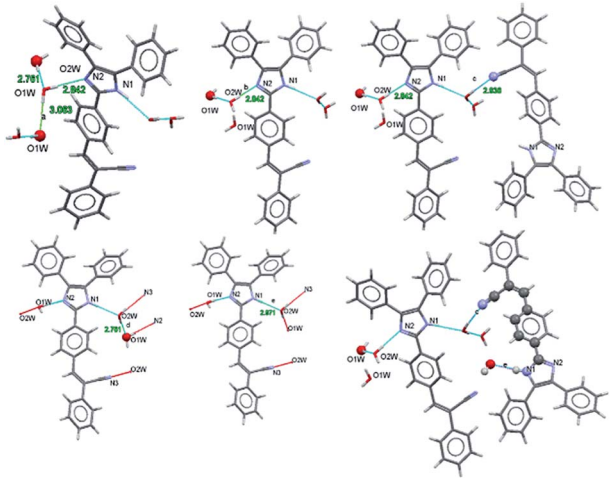

Fig. 4 Intermolecular motif formed interaction shown with a bond distance (Å). Chain motif and atoms involved in chain motif formation are shown in ball stick form.

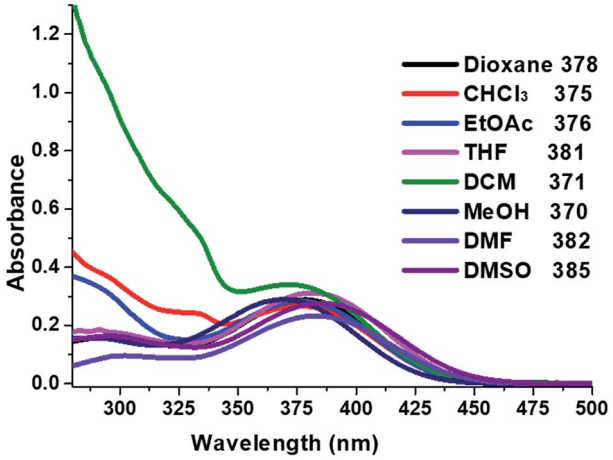

Fig. 5 Absorption spectrum of compound 2 with various solvents.

dimethyl sulfoxide (DMSO) (polar aprotic solvents). UV-Vis absorption maxima (λ_{abs}), extinction coefficients (ε) and optical band gap (E_{gap}) are listed in Table 3. The absorption spectra of compound **2** (Fig. 5), shows two maxima absorption, one in the range of 370–385 nm due to the π–π* transition. The mild band at 281–305 nm in the higher energy, (λ_{abs} 300 nm) was assigned to n–π* transition of the imidazole moiety.[49–51] The absorption bands of compound **2** observed when the solvent polarity increases from 1,4-dioxane to DMSO. With increasing polarity of aprotic solvents such as 1,4-dioxane (378 nm) < THF (381 nm) < DMF (382 nm) < DMSO (385 nm). However, there is a blue shift slightly (15 nm) observed for the protic solvent (MeOH). Non-polar solvents (dioxane < THF < DCM) showed higher molar extinction coefficient (ε) value than polar aprotic solvents (DMF, DMSO) and protic solvent (MeOH) (Table 4).

The optical band gap (E_{gap}) for compound **2** was estimated from the absorption spectrum edge using the absorption on set[52,53] (see Fig. S3 in ESI†). The calculate of E_{gap} values for the absorption band in range of 370 to 385 nm are summarised in Table 3. The non-polar aprotic solvents (dioxane, $CHCl_3$ THF, DCM) gave E_{gap} value increased from 2.78 to 2.82 eV (371 nm to 381 nm). In the case of the polar aprotic solvents (DMF, DMSO) the E_{gap} values are 2.79 eV, 2.77 eV respectively, whereas protic solvent (MeOH) was 2.73 eV. The difference could be an indication of the intermolecular hydrogen bond or interaction with imidazole moiety. These results are agreed with the solid-state intermolecular interactions to the solvent.

2.4 Photoluminescence studies

The photoluminescence (PL) study of the compound **2** in the selected solvents which are followed in the UV-Vis absorption study. The emission λ_{max} values are listed in Table 4 and the graph shown in Fig. 6. The compound **2** showed a red-shift with the increasing solvent polarity. Here we noticed that the solvent effect was stronger in emission compared to the absorption study, 503 nm to 568 nm as follow: dioxane (503 nm), $CHCl_3$ (502 nm), EtOAc (515 nm), THF (520 nm), DCM (523 nm). But there are longer shifts towards to longer wavelength in the case of polar protic solvents: MeOH (554 nm) and aprotic solvents DMF (559 nm), and DMSO (568 nm). In the same solvents, the quantum yield[54] was calculated to evaluate the effect of solvent, (solvatochromic effect). The calculated quantum yield[54] of the compound **2** is listed in Table 4.

Table 3 The data of absorbance for the compound 2 in the different solvents

Solvent	Dielectric constant	λ_{abs1} (nm)	λ_{abs2} (nm)	ε^a ($\times 10^{-4}$) (M^{-1} cm^{-1})	E_{gap}
1,4-Dioxane	2.25	300	378	3.337	2.82
$CHCl_3$	4.81	297	375	3.088	2.78
EtOAc	6.02	293	376	3.284	2.78
THF	7.58	305	381	3.607	2.78
DCM	8.93	281	371	3.938	2.82
MeOH	32.7	290	370	2.878	2.73
DMF	36.7	300	382	2.689	2.79
DMSO	46.7	297	385	3.202	2.77

[a] λ_{abs} = maximum absorption wavelength, $c = 2.5 \times 10^{-5}$ mol L^{-1}; ε = maximum molar absorption coefficient (M^{-1} cm^{-1}); E_{gap} = optical band gap derived from onset wavelength of the UV-Vis absorption spectra.

Table 4 The data of emission for the compound 2 in the different solvents[a]

Solvent	Dielectric constant	λ_{em} (nm)	Stoke shift (cm^{-1})	Φ_F
1,4-Dioxane	2.25	503	6574	0.10
$CHCl_3$	4.81	502	6746	0.07
EtOAc	6.02	515	7178	0.16
THF	7.58	520	7016	0.10
DCM	8.93	523	7833	0.21
MeOH	32.7	554	8976	0.11
DMF	36.7	559	8289	0.17
DMSO	46.7	568	8368	0.20

[a] λ_{em} = maximum emission wavelength, $c = 2.5 \times 10^{-5}$ mol L^{-1}; Φ_F = quantum yield measured by using fluorescein in 0.1 mol L^{-1} NaOH as standard.

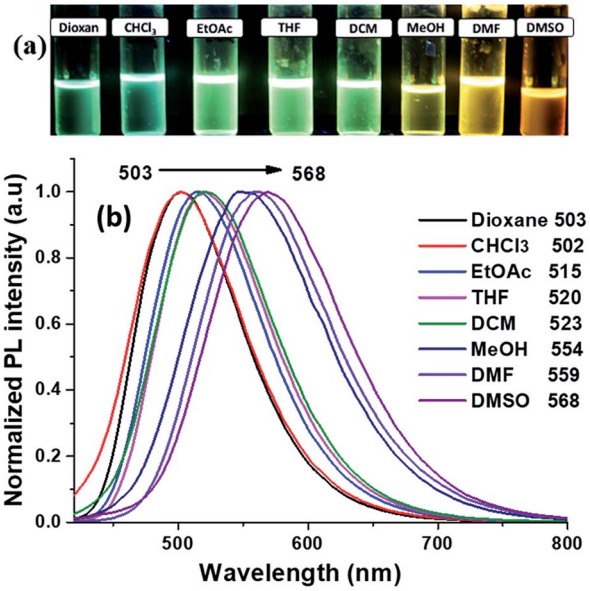

Fig. 6 (a) Solvatochromism (b) normalized emission spectra of compound **2** in several solvents.

The compound **2** exhibited a highest quantum yield value of 0.21 and 0.20 in DCM and DMSO respectively, whereas it is found to be lowest value of 0.07 in $CHCl_3$. These results are indicated solute and solvents interaction leads to change in the transition state which was responsible for the shift in the emission maxima.

For optical properties, solvents play an important role because it stimulates major changes in the position, intensity and shape of the absorption and emission bands.[55] The effect of solvent polarity on emission spectra is shown in Fig. 6a, a solvatochromic shift from green to yellowish orange was clearly visible upon UV irradiation. Compound **2** exhibited positive solvatochromism effect confirmed by the red-shift (66 nm) with increasing the polarity of the solvents and Fig. S1† showed the variation in the emission wavelength with different solvents polarity. The interaction of compound **2** with different polar solvents is mostly stabilized by the local excited states and thus lead to the bathochromic emission.[56] Stokes shift was calculated for the different the solvents and the values are obtained in the range of 6574–8368 cm^{-1} (Table 4), accordingly, the Stokes shift values are significantly increased with increasing the solvent polarity which indicated the presence of different charge distribution in the excited state (S_1) as compared to ground state (S_0). Here, phenylacrylonitrile part introduced in the imidazole derivative was the responsible for the more Stokes shift value when compare to the simple lophine (6513 cm^{-1})[20] By plotting the Stokes shifts ($\Delta\nu$) against the solvent polarity parameter Δf (ε, n), show approximately a linear relationship according to the Lippert–Mataga plot for the compound **2** (Fig. S2, ESI†). The change of the solvent polarity indicated the enhancement or diminished the electron density in the structure, as well as the intermolecular charge transfer (ICT) due to the strong interaction with the solvent.

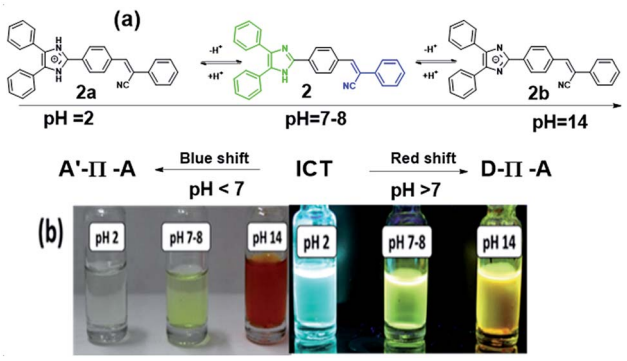

Fig. 7 (a) Plausible mechanism of protonation and deprotonation of compound **2** with different pH. (b) Halochromic effect of the compound **2**.

2.5 The effect of pH on absorption and emission spectra

There is one basic centre in the compound **2**, *i.e.*, imidazole NH group. As mentioned above both absorption and emission spectra showed a bathochromic shift in a polar aprotic solvent. To study the effect of pH on the absorption spectrum of compound **2** and to understand the effect of the electronic density on the π-conjugated through the donor to acceptor part. Fig. 7a shows the proposed mechanism of equilibrium between protonation at pH = 2 and deprotonation at pH = 14 of compound **2** in 5 mL of solvent's mixture THF–water (1 : 1). The experiments were carried out using solutions diluted with HCl and NaOH. Fig. 7b shows appearance of the solutions under normal and UV illumination.

The maxima absorption wavelength as free nitrogen forms of compound **2** appeared at 305 and 381 nm, which corresponding to the n–π* and π–π* transition respectively (Fig. 8a) and exhibit a high molar extinction coefficient (36 070 M^{-1} cm^{-1}). When increased the hydrogen ion concentration, (pH = 2), the cation species **2a** is formed due to the protonation of the nitrogen atom and the absorption attribute to the n–π* transition vanished, as well as the absorption band due to π–π* transition moves toward to blue region (23 nm) as compared to the neutral compound **2**. The formation of species **2a** observed by a colour change from greenish yellow to colourless in the visible light (Fig. 7b). The blue shift was obtained due to absence of lone pair in the imidazole which in turn to prevent the charge transfer and acts as acceptor (A). However, at a low concentration of hydrogen ion the bands appeared at 384 nm, and a new broad band was appeared at 467 nm as compared to

Table 5 The data of absorption, emission and spectroscopic determined E_{gap} for the compound **2** in the THF–H_2O mixture at the different pH values[a]

Medium	pH	λ_{abs} (nm)	λ_{em} (nm)	Φ_F	E_{gap} (eV)
Acidic	**2a**	357	476	0.07	2.99
Neutral	**2**	305, 381	530	0.10	2.81
Basic	**2b**	308, 384, 467	546, 671	0.15	2.19

[a] λ_{abs} = maximum absorption wavelength, $c = 1.0 \times 10^{-3}$ mol L^{-1}; λ_{em} = maximum absorption wavelength, $c = 1.0 \times 10^{-3}$ mol L^{-1}; E_{gap} = optical band gap derived from onset wavelength of the UV-Vis absorption spectra.

the neutral species **2** (Fig. 8a). At pH = 7 to 12, the absorption wavelength for n–π* and π–π* transition was almost the same. Further, with the decreasing of the hydrogen ion concentration, (*i.e.*) pH = 11 to 14, the species **2b** was detected when the colour changes of the greenish-yellow solution to reddish-orange. The absorption maxima for the solution (species **2b**) appeared at 308, 384 and 467 nm and corresponding to the n–π*, π–π* and possibility of inter- and intra-molecular charge transfers, respectively. Theses red shifts appeared due to great extent of intramolecular charge transfer (ICT) from donor to acceptor.[57] The lone pair electron of the anionic species (D) **2b** was showed more contribution in the CT compared to the lone pair electron of the neutral species **2**.

The fluorescence spectra of compound **2** at different pH are shown in the Fig. 8b. The species **2a** (pH = 2) showed sharp band at 476 nm with a shift to higher energy region of 54 nm compare to the neutral species **2**. In the acidic medium (pH = 2), it is possible that due to protonation of imidazole part generating a positive charge **2a** and it was reducing the donating character in the structure and presents a strong pull–push effect more than in neutral species **2** (*i.e.*, A′–π–A structural motif), which observed through the emission changing the colour from fluorescence greenish-yellow to cyan (Fig. 7b).

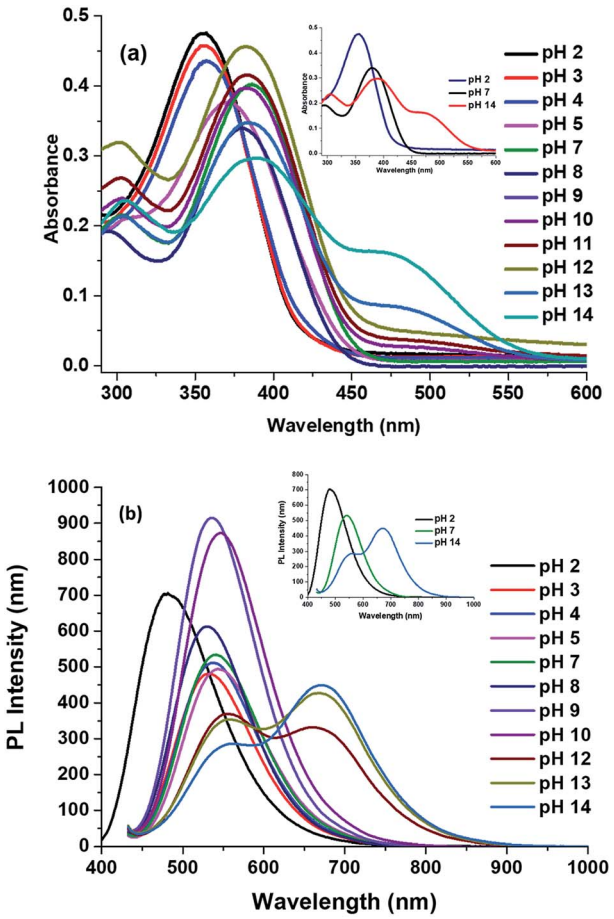

Fig. 8 (a) Absorption (b) emission spectra of compound **2** at different pH.

The emission spectra of compound **2** at pH = 8–11, the band was moved to lower energy from 520 nm to 548 nm, but the band is broad with emission from 500 nm to 700 nm with increasing intensity. It shows the charge transfer take place in the initial level (*i.e.*, D–π–A structural motif). According to the measurement, after the pH 12–14, the species **2b** was formed which is not making more changes in emission but it could be fine-tuned from greenish-yellow to dark reddish-violet (Fig. 7b). The emission maxima moved from 546 to 561 nm with decreasing intensity meanwhile another peak appeared at 659 nm and it shifted to 671 nm with increasing intensity (Fig. 8b). It indicated that N-3 position of the imidazole ring was deprotonated, and it can induce the intramolecular charge transfer (ICT), between the anion nature of the imidazole ring (D) to phenylacrylonitrile (A).

The alteration of [H^+] ion concentration can alter push–pull nature (ICT) between the donor to acceptor. It was well correlating with optical band (E_{gap}) values, calculated by absorption onset (Fig. S4 in ESI†). The E_{gap} values of species **2**, **2a** and **2b** were obtained as 2.81, 2.99 and 2.19 eV respectively (Table 5). The E_{gap} values were changed through the modifying the [H^+] ion concentration. The E_{gap} values are higher in acidic medium (pH = 2) than the basic medium (pH = 14). This indication observed in the absorption maxima by blue shift at the acidic medium whereas red shift occurred at the basic medium compared to the neutral condition. These results indicated the compound **2** was able to act as D–π–A or A′–π–A structural motif based on the pH nature and hence it showed a promising candidate for the pH sensor.

2.6 Solid state photoluminescence

From our group previous experiences, phenyl acrylonitrile derivatives (α-cyanostilbene) exhibited the good solid-state emission which used to make for a better organoelctronic device. In order to examine how imidazole based phenylacrylonitrile showed its solid-state emission properties in the thin film (TF) and powder form. Thin films were deposited onto cleaned glass substrates by two process, one is the spin coating method (solution) and other is the thermal vacuum deposition method. Absorption and emission spectra of the thin film and powder are shown in Fig. 9. The powder showed a spectrum with a broad shape (420 nm), but in thin film showed a defined shape with λ_{abs} value at 388 nm. The powder form showed a broadening shape of the absorption maxima may be due to the intermolecular interaction or intramolecular interaction took place. The absorbance and emission spectra are shown in Fig. 9 and corresponding data are listed in Table S6.† The emission spectra of the powder and film showed λ_{em} band around 563 nm and 540 nm respectively. The quantum yield of the powder was found to be 16% and, in the solution is 21%.

The surface morphology of the films by solution-processed and vacuum evaporation are compared in the Fig. 10. The evaporation process leads to form morphology with agglomerates of about 300 nm and the morphology by solution process showed an arrangement alignment as herringbone. Optical properties, absorption and emission were like the solution-

processed films. The thin films prepared by high vacuum deposition were exposed to HCl, H_2SO_4, HNO_3 vapours. After few minutes, the sample exposed to HNO_3 only showed the transformation.

It was followed by absorption measurements and exposed the films under UV lamp was examined to see the change of the fluorescence. Fig. 11a showed a pure film for the reference and Fig. 11b showed exposed to HNO_3 vapor film. It can be seen the blue-shift in fluorescence emission, at same wavelength as the compound **2** in solution at pH = 2. The observed phenomenon also was reversible, because after 4 days the films come to the original colour and the fluorescence, Fig. 11c.

Absorption (solid line) and emission (short dashed line) spectra were measured and shown in the Fig. 12. After exposure both spectra showed a hypsochromic effect, for absorption a maximum absorption showed a shift of 37 nm while the emission shifts to 52 nm. As mentioned above, the change in fluorescence was reversible, Fig. 12, showed the absorbance and fluorescence spectra for the compound in thin film exposed to HNO_3 and kept at normal atmosphere for four days. Interestingly, the emission is like the original one (λ_{PL} = 545 nm). However, the absorbance remains as like the exposed film. It could be the transformation of the organic compound film was not completed. However, the experiment show that it is possible tuning the fluorescence as well as the application as vapor senor fluorescence (Fig. 12).

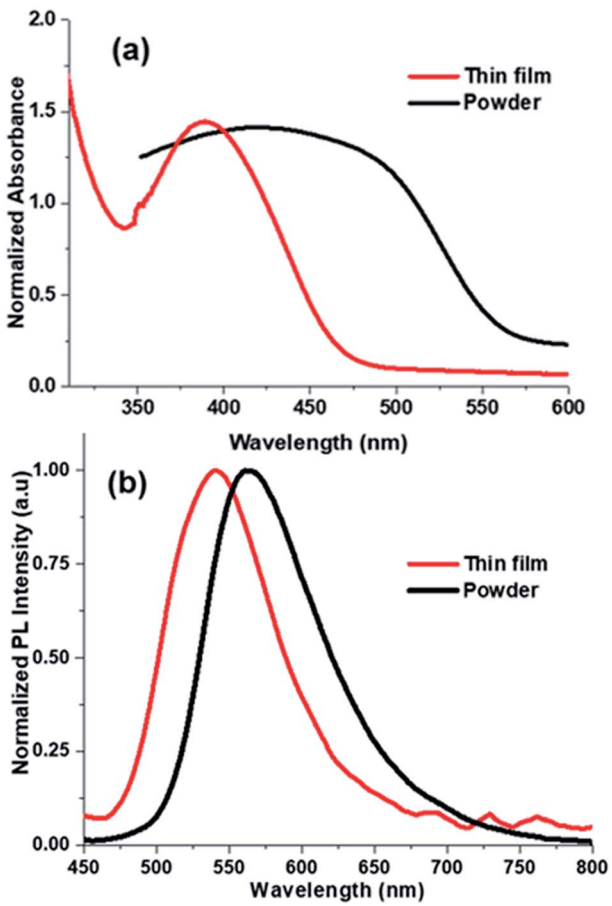

Fig. 9 (a) Absorption and (b) emission spectra of compound **2** in the powder and thin film.

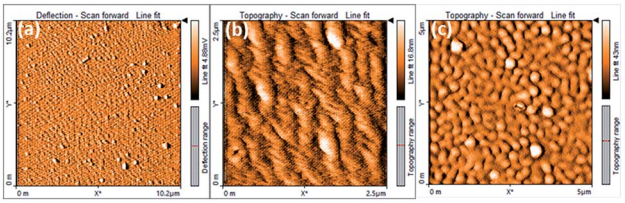

Fig. 10 (a) and (b) AFM image of the compound **2** thin film by solution process and (c) morphology image of evaporated films.

For making the OLED of compound **2** using the vacuum deposition film and its photo luminance (PL) and electro luminance (EL) spectra are shown in Fig. 13a. The wavelength of maximum emission was about 550 nm. The *J–V* curve for OLED is shown in Fig. 13b, the threshold voltage was about 4 V, the inset shows a picture for OLED. The average luminance for devices was about 450 cd m^{-2}. It indicates that compound **2** had promising candidate for an electronic device as well as the vapour sensor device.

2.7 Theoretical calculation

To understand the electronic properties of compound **2**, we carried out the TD-DFT calculations in the gas phase and solution state (1,4-dioxane, chloroform, ethyl acetate, THF, DCM, methanol, DMF, and DMSO). It's corresponding to the cation and anion structures with B3LYP/6-311++G (d, p) level of theory. The calculated absorption wavelength (λ_{abs}), oscillator strengths (f), and major orbital transitions (in %) for compound **2** is presented in Tables S8 and S9 ESI.† The most important the Frontier molecular orbital (FMO) (Highest Occupied Molecular Orbital, HOMO and Lowest Unoccupied Molecular Orbital, LUMO) are presented in Fig. 14. The computed absorption of the compound **2** in gas phase and in the solutions state showed around 450 nm. These values may be due to the intramolecular charge transfer (H → L transition with 100%) arise from the electron pulling nature of phenylacrylonitrile moiety (acceptor). This CT was observed in the absorption spectrum of powder form but did not observe in the solution and TF (Fig. 9a). The second absorption peaks in the both states showed around 340 nm are corresponding to π → π* transition (H − 1 → L with 86–100%). Another weak transition around 319–330 nm, it belongs to n → π* transition (H → L + 1 with 90–100%). On the other hand, when increasing the solvent polarity, the computed λ_{max} value showed slightly blue shift as like experiment results. To understand the effect of pH on molecular structure, we computed to the absorptions for the compound **2** in the form of

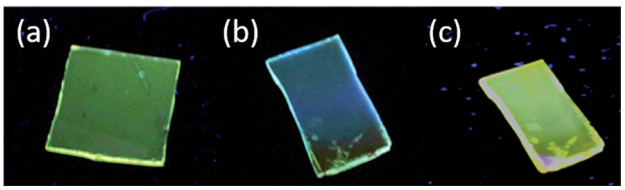

Fig. 11 (a) Thin film (TF) as reference (b) exposed to HNO_3 (c) exposed TF after 4 days.

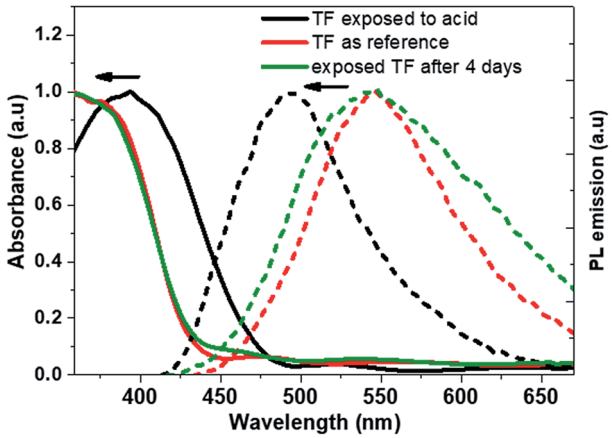

Fig. 12 Absorption and emission spectra of compound **2** in thin film (TF).

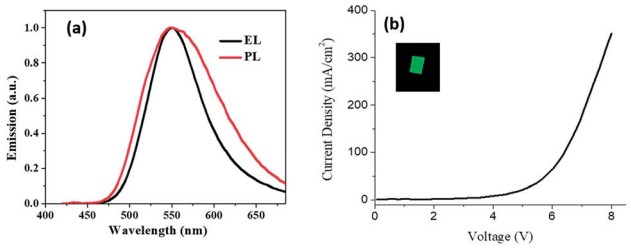

Fig. 13 (a) Photoluminescence and electroluminescence spectra of thin film and OLEDs respectively. (b) Electrical characteristics *J*–*V* for OLEDs (the inset shows an OLED picture).

the cation and anion environment (Table S9†). From the results, the H → L transition went to blue shift (440 nm in gas and 417 nm in THF), for the cationic environment whereas for the anionic environment absorption moved to a strong red shift (at 582 nm in gas and 562 nm in THF). These results are matched with in the pH experimental values. In order to understand for the strong Stokes shift observed at pH 14. It was performed the HOMO–LUMO analysis for the compound **2** at neutral, cation and anion environment. The HOMO and LUMO energy level of compound **2** (at neutral) was of −5.67 eV and −2.59 eV respectively, and it's ΔE_{gap} of 3.08 eV. These results were closer to the experimental results of the CV measurements (Fig. S5,† HOMO is −5.677 eV and LUMO is −2.868 eV; ΔE_{gap} of 2.81 eV). It noted that the HOMO and LUMO of cation is more stabilized with 3.05 eV than the neutral molecule. Whereas HOMO of anion is less stabilized with 3.60 eV and 2.69 eV for LUMO of anion than neutral molecule. These variations in energy level of FMO is might be reason for the blue shift absorption and emission in acidic and red shift in the basic medium.

To recognise that the origin of intramolecular charge transfer in the title molecule, we carried out the NBO analysis for neutral, cation and anionic state of the molecule (Tables S8 and S9†). The result suggested that the whole molecule involved in the intramolecular charge transfer process. Briefly, the phenylacrylnitrile moiety in the neutral molecule is predominately involved in the charge transfer process with the strong stabilization energy. Whereas the imidazole moiety is strongly or moderately involved in the intramolecular charge transfer process with moderate stabilization energy in the cation and anion environment. The NBO analysis suggested that the phenylacrylonitrile moiety acts as a strong electron withdrawing moiety and it enhanced the intramolecular charges transfer along the whole molecule.

Finally, the optoelectronic calculations with the aid Schrödinger programme, we compute the oxidation potential and reduction potential values of compound **2** help us to see that the compound to loose/gain electrons. From the CV values are of 1.455 eV and −1.354 eV respectively, that compared with the calculated are closer for the reduction potential with a difference −0.0461 eV between the calculated and experimental. That is an indication that the compound **2** acta more acceptor than donating. The presence of the electro withdrawing CN group in the molecule is responsible for an oxidation potential higher than similar molecule imidazole groups.[58] In the Table S5,† exhibits hole and electron reorganization energies (HRE and ERE). It is worth to notice that the reorganization energy (RE) is one of the parameters governing the hopping rate. It has long been recognized that HRE and ERE are closely related to the geometries of cation and anion states. In fact, the RE is defined as the energy difference between the charged and neutral systems. The molecules with small RE possess high carrier mobility and these energies are in proportion to the deformation of the geometries in charge transfer process. In compound **2** the HRE is 0.1064 smaller than the ERE indicating a smaller geometrical deformation upon electron injection compared to hole injection. This value is remarkably small, indicated that the hole extraction potential of 6.368 eV, which demonstrates that the injection of hole into compound **2** is slightly easier. On the contrary, compound **2** has maximum electron extraction potential of −1.2032 eV, indicating that the injection of electron into the compound **2** becomes much difficult.

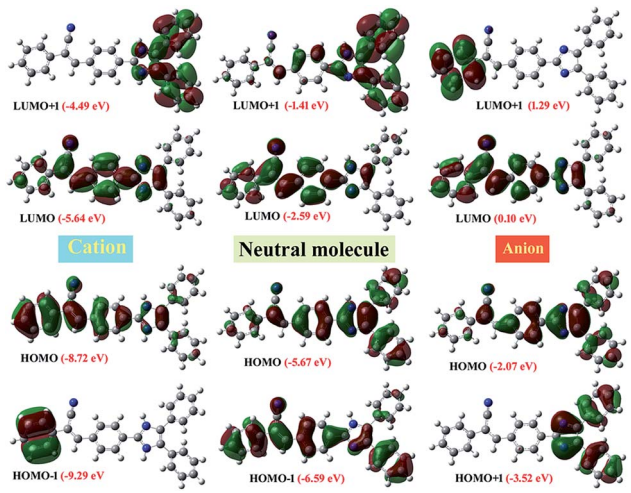

Fig. 14 The HOMO–LUMO diagram of the compound **2** in neutral, acidic and basic condition.

3. Conclusion

In summary, it was designed a novel Imidazole based luminogenic compound was characterized by SCXRD, FT-IR, ^{1}H NMR, ^{13}C NMR and EIMS. We investigated the photophysical properties of compound **2** in solution state with various solvents and in the solid states (TF and powder). In the solution state, it showed the positive solvatochromic behaviour and it had a solid-state emission too. Furthermore, by varying the pH medium to observe the intramolecular charge transfer in solution and solid state (TF) and it resulted the halochromic behaviour. The phenyl rings of imidazole moiety trigged by protonation and deprotonation of the imidazole group and its reason for the electronic transition (ICT) *via* C-2 phenyl ring to the acceptor of phenyl acrylonitrile group. Based on that compound **2** can be used as pH sensor for solution and vapor medium. Optical band gap values are estimated from cyclic voltammetry and the absorption onset. Overall, compound **2** can able to act as D–π–A as well as A′–π–A based on the pH nature. In addition, the compound was used as emitting layer in OLEDs with acceptable performance. TD-DFT computations and the energy levels of FMO are very closer to the experimental results and it aid to give an insight idea to support the studies. Therefore, it can act as a new multi-functional material for the field of sensor and organo-electronic application.

4. Experimental section

4.1 Materials and instruments

Benzil(1,2-diphenylethane-1,2-dione), phenylacetonitrile, 4-formylbenzaldehyde (1,4-terephtaldehyde) and ammonium acetate were acquired from Aldrich Chemical Co. and Fermont. The reagents and solvents were used as received without any additional purification. Melting points were measured with an SEV (0–300 °C) apparatus and were reported as uncorrected values. IR spectra of the products were recorded on a Vertex (model 70, Bruker Optics, Germany) 750 FT-IR spectrophotometer by attenuated total reflectance (ATR). ^{1}H NMR and ^{13}C NMR spectra were obtained in DMSO-d_6 on a Bruker 500 MHz NMR spectrometer. The electron ionization (EI) spectra were acquired on a Jeol MStation 700-D mass spectrometer (Jeol USA, Peabody, MA). Absorbance and emission (UV-Vis and PL). The absorbance spectra were measured using a spectrometer Cary 300 (Agilent) equipped with a deuterium and halogen lamp. Emission spectra (PL) were acquired with a QE-Pro-FL (Ocean Optics, Dunedin, FL) an UV-Lamp Mineral Light with emission at 401 nm was used as excitation source. *I–V* curves were acquired with a source-meter Keithley 2450. Electroluminescence spectra were recorded with an Ocean Optics spectrometer. The morphology and thickness were analyzed using atomic force microscopy (AFM) with the microscope EasyScan2 from Nanosurf operating in contact mode under ambient conditions. This has a maximum square scanning area of 110 μm. The adjustment of pH solutions was achieved through the addition of NaOH or HCl solutions and monitored with the aid of Metrohm 716 DMS Titrino Titrator pH meter using buffers of pH 4.0 and pH 9.2 as calibrants. Cyclic Voltammetry (CV) measurements were carried out with a potentiostat (PGSTAT128N), using a three-electrode cell assembly comprising Ag/Ag$^+$ in a 3 M solution of KCl as a reference electrode, a platinum wire (ϕ = 0.2 mm) as the working electrode, a 0.1 M solution of tetrabutylammonium hexafluorophosphate (TBAFP6) CH_2Cl_2 as a supporting electrolyte and a platinum wire as the counter electrode. Ferrocene was used as an external standard. The scanning rate was 50 mV s^{-1}.

Single crystal X-ray diffraction (SCXRD). All reflection intensities were measured at 110(2) K using a SuperNova diffractometer (equipped with Atlas detector) with Cu Kα radiation (λ = 1.54178 Å) under the program CrysAlisPro (Version CrysAlisPro 1.171.39.29c, Rigaku OD, 2017)[59] The same program was used to refine the cell dimensions and for data reduction. The structure was solved with the program SHELXS-2018/3 (Sheldrick, 2018) and was refined on F2 with SHELXL-2018/3 (Sheldrick, 2018). Analytical numeric absorption correction using a multifaceted crystal model was applied using CrysAlisPro. The temperature of the data collection was controlled using the system Cryojet (manufactured by Oxford Instruments). The H atoms were placed at calculated positions (unless otherwise specified) using the instructions AFIX 43 with isotropic displacement parameters having values 1.2 Ueq. of the attached C atoms. The H atoms attached to N1, O1W and O2W were found from difference Fourier maps, and their coordinates were refined pseudo freely using the DFIX instruction to keep the N–H, O–H and H⋯H distances within acceptable ranges. The structure is ordered.

OLEDs: thin film and devices fabrication. For OLEDs ITO/glass substrates with 5–15 Ω per square were purchased from Delta Technologies. Poly(3,4-ethylenedioxythiophene) polystyrene sulfonate (PEDOT:PSS) (Clevios PVP AI4083) was obtained from Heraeus–Clevios and this compound acts as hole transport layer. Ca and Ag used as cathode were acquired from Sigma Aldrich. Substrates, glass for films and glass/ITO for OLEDs were cleaned with ethanol in an ultrasonic bath and rubbed with alcohol wetted cotton; after this procedure, substrates were dried with clean and dry air and kept at 85 °C, over 12 h. Before deposition of the organic layers, the substrates were treated with plasma-oxygen by 5 min. For OLEDs, PEDOT:PSS was deposited by spin coating and annealed at 120 °C by 15 min in air, thickness was about 45 nm. Then, substrates were transferred to an evaporation chamber and 100 nm of the fluorescent compound was evaporated at 0.5 Å s^{-1}, the chamber pressure was 2 × 10^{-6} Torr. A double layer of calcium (50 nm) and silver (100 nm) was used as cathode and evaporated sequentially after the organic layer. The thickness of the organic layer was measured through Atomic Force Microscopy (AFM) Nanosurf EasyScan. The emissive area of samples was of 9 mm2. For recording, the *I–V* curves a source-meter Keithley 2450 was used. The photoluminescence, electroluminescence (EL) and luminance were measured with an Ocean optics USB4000 spectrophotometer, calibrated with the HL-3P-CAL lamp.

Quantum chemical calculations. All the quantum chemical calculations were performed with the Gaussian 09 program.[60] The constrains free optimization was carried out by using M06-

2X[61,62] cc-PVTZ level of theory with Grimme's D3 dispersion corrections.[63] The selection of M06-2X and basis set has been made on our earlier studies.[64–69] The vibrational frequency was calculated for the optimized geometry in vacuum and solvent phases to determine the energy minima on the potential energy surface and were found to have no negative frequencies. All the solution phase calculations were carried out by using the conductor-like polarizable continuum model (CPCM).[70,71] Time-dependent DFT (TDDFT)[72] is used to calculate the absorption properties from the optimized geometries All the absorption values are not comparable with experimental result.

Optoelectronic calculation. Optoelectronic calculation for compound **2** was carried out in the materials science suite in the Schrödinger program.[73] The materials science suite provides very accurate optoelectronic properties standard materials like $Ir(ppy)_3$ and AlQ_3 compounds.[74] For this calculation it was used a gas phase optimized geometry of compound **2** which was obtained from jaguar suite in the Schrödinger program,[73] and the optimization process was carried out with MIDIX basis set with gradient-corrected correlation functional of B3LYP.[75–77] To confirm the proper convergence to minima, it was computed the vibrational frequencies with same level of theory to confirm that no negative frequencies presented.

4.2 Synthesis of 4-(4,5-diphenyl-1*H*-imidazol-2-yl) benzaldehyde (1)

A mixture of 4-formylbenzaldehyde (500 mg, 3.730 mmol), benzil (627 mg, 3.730 mmol), NH_4OAc (3.45 mg, 44.76 mmol) in acetic acid (50 mL) was refluxed for 5 hours, and then cooled to room temperature. The reaction mixture was poured into the ice-cold water and allowed to be left for 1 h, filtered, and the yellow precipitate was washed with water. The crude product was suspended in EtOAc and filter it. The filtrate was concentrated by evaporation and the solid product washed with 5% (EtOAc : Hex). The product was identified by their spectral data.[78] Pale yellow solid, yield: 42%, mp 233–235 °C (lit. [72] 233–235 °C); ^{1}H NMR (500 MHz, DMSO) δ 13.04 (s, 1H), 10.04 (s, 1H), 8.31 (d, J = 8.3 Hz, 2H), 8.02 (d, J = 8.5 Hz, 2H), 7.55 (dd, J = 16.8, 7.4 Hz, 4H), 7.47 (t, J = 7.4 Hz, 2H), 7.42 (d, J = 7.2 Hz, 1H), 7.33 (t, J = 7.5 Hz, 2H), 7.26 (d, J = 7.2 Hz, 1H). IR (KBr, cm^{-1}): 1696(–CHO), 1605(–C=NH–), 1309 (–C–N).

4.3 Synthesis of (*Z*)-3-(4-(4,5-diphenyl-1*H*-imidazol-2-yl) phenyl)-2-phenylacrylonitrile (2)

A mixture of the compound **1** (50 mg, 0.1542 mmol), 2-phenyl acetonitrile (18 mg, 0.1542 mmol), KOH (1.7 mg, 0.03084 mmol) in MeOH (2 mL) was refluxed for 6 hours to get compound **2** as a yellow solid. After completion, the reaction mixture was dried, added a water to filter the resulting precipitate. For neutralize the precipitate, water was used to wash. In order to recrystallization, briefly, 0.05 g of the title compound was dissolved in 20 mL commercial MeOH, heated at 85 °C for 2 h, filter it and allowed to evaporate the filtrate slowly at room temperature. The expected product was obtained as crystal. Yellow solid, yield: 65%, mp. 244–246 °C; ^{1}H NMR (500 MHz, CDCl3, δ) 9.92 (s, 1H, –NH), 7.95 (d, 2H, J = 10 Hz, ArH), 7.90 (d, 2H, J = 10 Hz, ArH), 7.59–7.58 (m, 4H, ArH), 7.47 (s, 1H, =CH), 7.40–7.24 (m, 11H); 13C NMR (100 MHz, CDCl3, δ) 145.0, 141.6, 134.4, 133.6, 131.6, 129.9, 129.1, 128.9, 128.4, 127.9, 126.0, 125.5, 118.2, 111.4; IR (KBr, cm^{-1}) ν: 3301(NH), 2211 (–C≡N), 1593(–CH=N–), 1363(–C–N–); MS (ESI): [M$^+$] calculated for $C_{30}H_{21}N_3$ 423.17, found 423.0, 154 (100%), 136 (72%), 307 (21%)

Conflicts of interest

There are no conflicts to declare.

Acknowledgements

The authors wish to express their gratitude to VIEP-BUAP (project PEZM-NAT16-G), to project fellowship-PRODEP-SEP 511-6/17-11066 and 511-6/18-16257, to Maxime Siegler for the X-ray determination, Laboratorio Nacional de Supercómputo del Sureste (LNS-BUAP) to perform the calculations as well as to Vladimir Carranza for technical assistance with mass spectrometry.

Notes and references

1 H. Schill, S. Nizamov, F. Bottanelli, J. Bierwagen, V. N. Belov and S. W. Hell, *Chem.–Eur. J.*, 2013, **19**, 16556–16565.
2 D. Huang, T. Zhao, W. Xu, T. Yang and P. S. Cremer, *Anal. Chem.*, 2013, **85**, 10240–10248.
3 X.-D. Liu, Y. Xu, R. Sun, Y.-J. Xu, J.-M. Lu and J.-F. Ge, *Analyst*, 2013, **138**, 6542–6550.
4 G. Gryn'ova and C. Corminboeuf, *J. Phys. Chem. Lett.*, 2018, **9**, 2298–2304.
5 S. Sasaki, G. P. C. Drummen and G. Konishi, *J. Mater. Chem. C*, 2016, **4**, 2731–2743.
6 C. Wu, J. Wei, D. Tian, Y. Feng, R. H. Miller and Y. Wang, *J. Med. Chem.*, 2008, **51**, 6682–6688.
7 G. Cheng, D. Wenyue, Y. Liang, L. Ying, Z. Zhongbo, L. Dan and M. Yuguang, *Adv. Mater.*, 2012, **24**, 2413–2417.
8 J. S. Wilson, M. J. Frampton, J. J. Michels, L. Sardone, G. Marletta, R. H. Friend, P. Samori, H. L. Anderson and F. Cacialli, *Adv. Mater.*, 2005, **17**, 2659–2663.
9 P. Zrazhevskiy, M. Sena and X. Gao, *Chem. Soc. Rev.*, 2010, **39**, 4326–4354.
10 H. Sasabe and J. Kido, *Chem. Mater.*, 2011, **23**, 621–630.
11 D. Ding, J. Liang, H. Shi, R. T. K. Kwok, M. Gao, G. Feng, Y. Yuan, B. Z. Tang and B. Liu, *J. Mater. Chem. B*, 2014, **2**, 231–238.
12 M. Klikar, P. Solanke, J. Tydlitát and F. Bureš, *Chem. Rec.*, 2016, **16**, 1886–1905.
13 W. Aigner, O. Bienek, B. P. Falcão, S. U. Ahmed, H. Wiggers, M. Stutzmann and R. N. Pereira, *Nanoscale*, 2018, **10**, 8042–8057.
14 S. Jhulki and J. N. Moorthy, *J. Mater. Chem. C*, 2018, **6**, 8280–8325.
15 P. Kan-Yi and L. Bin, *Adv. Funct. Mater.*, 2009, **19**, 277–284.
16 T. P. I. Saragi, T. Spehr, A. Siebert, T. Fuhrmann-Lieker and J. Salbeck, *Chem. Rev.*, 2007, **107**, 1011–1065.

17 A. Kundu, S. Karthikeyan, Y. Sagara, D. Moon and S. P. Anthony, *Phys. Chem. Chem. Phys.*, 2018, **20**, 27385–27393.
18 G. Wiethaus, J. M. Toldo, F. da Silveira Santos, R. da Costa Duarte, P. F. B. Gonçalves and F. S. Rodembusch, *Phys. Chem. Chem. Phys.*, 2019, **21**, 4408–4420.
19 Z. Fang, S. Wang, L. Zhao, Z. Xu, J. Ren, X. Wang and Q. Yang, *Mater. Chem. Phys.*, 2008, **107**, 305–309.
20 A. Hariharasubramanian and Y. D. Ravichandran, *RSC Adv.*, 2014, **4**, 54740–54746.
21 Y. Zhang, S.-L. Lai, Q.-X. Tong, M.-F. Lo, T.-W. Ng, M.-Y. Chan, Z.-C. Wen, J. He, K.-S. Jeff, X.-L. Tang, W.-M. Liu, C.-C. Ko, P.-F. Wang and C.-S. Lee, *Chem. Mater.*, 2012, **24**, 61–70.
22 H.-M. Zhang, W.-F. Fu, S.-M. Chi and J. Wang, *J. Lumin.*, 2009, **129**, 589–594.
23 J. Kulhánek and F. Bureš, *Beilstein J. Org. Chem.*, 2012, **8**, 25–49.
24 J. Jayabharathi, V. Thanikachalam, N. Srinivasan and M. V Perumal, *Spectrochim. Acta, Part A*, 2012, **90**, 125–130.
25 J. Mandal, P. Ghorai, P. Brandão, K. Pal, P. Karmakar and A. Saha, *New J. Chem.*, 2018, **42**, 19818–19826.
26 R. Bag, Y. Sikdar, S. Sahu, D. K. Maiti, A. Frontera, A. Bauzá, M. G. B. Drew and S. Goswami, *Dalton Trans.*, 2018, **47**, 17077–17085.
27 N. Fridman, M. Kaftory, Y. Eichen and S. Speiser, *J. Mol. Struct.*, 2009, **917**, 101–109.
28 M. Y. Berezin, J. Kao and S. Achilefu, *Chem.–Eur. J.*, 2009, **15**, 3560–3566.
29 K. Aggarwal and J. M. Khurana, *J. Photochem. Photobiol., A*, 2015, **307–308**, 23–29.
30 A. Safavi and M. Bagheri, *Sens. Actuators, B*, 2003, **90**, 143–150.
31 B. Kumari, S. P. Singh, R. Santosh, A. Dutta, S. S. Mallajosyula, S. Ghosal and S. Kanvah, *New J. Chem.*, 2019, **43**, 4106–4115.
32 L. Zhu and Y. Zhao, *J. Mater. Chem. C*, 2013, **1**, 1059–1065.
33 J. N. Zhang, H. Kang, N. Li, S. M. Zhou, H. M. Sun, S. W. Yin, N. Zhao and B. Z. Tang, *Chem. Sci.*, 2017, **8**, 577–582.
34 M. Martínez-Abadía, R. Giménez and M. B. Ros, *Adv. Mater.*, 2018, **30**, 1704161.
35 C. Dou, L. Han, S. Zhao, H. Zhang and Y. Wang, *J. Phys. Chem. Lett.*, 2011, **2**, 666–670.
36 R. Usman, A. Khan, M. Wang, Y. Luo, W. Sun, H. Sun, C. Du and N. He, *Cryst. Growth Des.*, 2018, **18**, 6001–6008.
37 M. Wykes, S. K. Park, S. Bhattacharyya, S. Varghese, J. E. Kwon, D. R. Whang, I. Cho, R. Wannemacher, L. Lüer, S. Y. Park and J. Gierschner, *J. Phys. Chem. Lett.*, 2015, **6**, 3682–3687.
38 M. J. Percino, V. M. Chapela, E. Pérez-Gutiérrez, M. Cerón and G. Soriano, *Chem. Pap.*, 2011, **65**, 42–51.
39 M. Castro, M. Percino, V. Chapela, M. Ceron, G. Soriano-Moro, J. Lopez-Cruz, F. Melendez, M. E. Castro, M. J. Percino, V. M. Chapela, M. Ceron, G. Soriano-Moro, J. Lopez-Cruz and F. J. Melendez, *Int. J. Mol. Sci.*, 2013, **14**, 4005–4029.
40 M. J. Percino, V. M. Chapela, L.-F. Montiel, E. Pérez-Gutiérrez and J. L. Maldonado, *Chem. Pap.*, 2010, **64**, 360–367.
41 Z.-Q. Yan, Z.-Y. Yang, H. Wang, A.-W. Li, L.-P. Wang, H. Yang and B.-R. Gao, *Spectrochim. Acta, Part A*, 2011, **78**, 1640–1645.
42 Y. Li, F. Li, H. Zhang, Z. Xie, W. Xie, H. Xu, B. Li, F. Shen, L. Ye, M. Hanif, D. Ma and Y. Ma, *Chem. Commun.*, 2007, 231–233.
43 B.-R. Gao, H.-Y. Wang, Y.-W. Hao, L.-M. Fu, H.-H. Fang, Y. Jiang, L. Wang, Q.-D. Chen, H. Xia, L.-Y. Pan, Y.-G. Ma and H.-B. Sun, *J. Phys. Chem. B*, 2010, **114**, 128–134.
44 F. H. Allen, O. Kennard, D. G. Watson, L. Brammer, A. G. Orpen and R. Taylor, *J. Chem. Soc., Perkin Trans. 2*, 1987, S1–S19.
45 K. Molčanov, I. Sabljić and B. Kojić-Prodić, *CrystEngComm*, 2011, **13**, 4211–4217.
46 O. V Dolomanov, L. J. Bourhis, R. J. Gildea, J. A. K. Howard and H. Puschmann, *J. Appl. Crystallogr.*, 2009, **42**, 339–341.
47 T. Steiner, *Angew. Chem., Int. Ed.*, 2002, **41**, 48–76.
48 M. Inoue and I. Hirasawa, *J. Cryst. Growth*, 2013, **380**, 169–175.
49 Z.-B. Cai, L. Bai, Y.-L. Pan, F.-F. Ma, S.-L. Li and Y.-P. Tian, *J. Photochem. Photobiol., A*, 2017, **346**, 194–205.
50 G.-C. Zheng, Z.-B. Cai, Y.-L. Pan, L. Bai, Y.-T. Zhou, S.-L. Li and Y.-P. Tian, *Tetrahedron*, 2016, **72**, 2988–2996.
51 M. J. Percino, M. Cerón, G. Soriano-Moro, M. E. Castro, V. M. Chapela, J. Bonilla, M. Reyes-Reyes and R. López-Sandoval, *CrystEngComm*, 2014, **16**, 8591–8604.
52 M. M. Duvenhage, M. Ntwaeaborwa, H. G. Visser, P. J. Swarts, J. C. Swarts and H. C. Swart, *Opt. Mater.*, 2015, **42**, 193–198.
53 J. C. S. Costa, R. J. S. Taveira, C. F. R. A. C. Lima, A. Mendes and L. M. N. B. F. Santos, *Opt. Mater.*, 2016, **58**, 51–60.
54 S. Dhami, A. J. De Mello, G. Rumbles, S. M. Bishop, D. Phillips and A. Beeby, *Photochem. Photobiol.*, 2018, **61**, 341–346.
55 M. J. Wirth, *TrAC, Trends Anal. Chem.*, 1982, **1**, 383–386.
56 R. Ghosh and D. K. Palit, *Photochem. Photobiol. Sci.*, 2013, **12**, 987–995.
57 A. O. Eseola, O. Adepitan, H. Görls and W. Plass, *New J. Chem.*, 2012, **36**, 891–902.
58 J. J. Guerard, P. R. Tentscher, M. Seijo and J. Samuel Arey, *Phys. Chem. Chem. Phys.*, 2015, **17**, 14811–14826.
59 G. M. Sheldrick, *Acta Crystallogr., Sect. C: Struct. Chem.*, 2015, **71**, 3–8.
60 M. J. Frisch, G. W. Trucks, H. B. Schlegel, G. E. Scuseria, M. A. Robb, J. R. Cheeseman, G. Scalmani, V. Barone, B. Mennucci, G. A. Petersson, H. Nakatsuji, M. Caricato, X. Li, H. P. Hratchian, A. F. Izmaylov, J. Bloino, G. Zheng, J. L. Sonnenberg, M. Hada, M. Ehara, K. Toyota, R. Fukuda, J. Hasegawa, M. Ishida, T. Nakajima, Y. Honda, O. Kitao, H. Nakai, T. Vreven, J. A. Montgomery, J. E. Peralta, F. Ogliaro, M. Bearpark, J. J. Heyd, E. Brothers, K. N. Kudin, V. N. Staroverov, R. Kobayashi, J. Normand, K. Raghavachari, A. Rendell, J. C. Burant, S. S. Iyengar, J. Tomasi, M. Cossi, N. Rega, J. M. Millam, M. Klene, J. E. Knox, J. B. Cross, V. Bakken, C. Adamo, J. Jaramillo, R. Gomperts, R. E. Stratmann, O. Yazyev,

A. J. Austin, R. Cammi, C. Pomelli, J. W. Ochterski, R. L. Martin, K. Morokuma, V. G. Zakrzewski, G. A. Voth, P. Salvador, J. J. Dannenberg, S. Dapprich, A. D. Daniels, O. Farkas, J. B. Foresman, J. V. Ortiz, J. Cioslowski and D. J. Fox, *Gaussian 09, Revis. B.01*, Gaussian, Inc., Wallingford CT, 2009.

61 Y. Zhao, N. E. Schultz and D. G. Truhlar, *J. Chem. Theory Comput.*, 2006, **2**, 364–382.

62 E. G. Hohenstein, S. T. Chill and C. D. Sherrill, *J. Chem. Theory Comput.*, 2008, **4**, 1996–2000.

63 S. Grimme, J. Antony, S. Ehrlich and H. Krieg, *J. Chem. Phys.*, 2010, **132**, 154104.

64 J. Percino, M. Cerón, P. Venkatesan, P. Ceballos, A. Bañuelos, O. Rodríguez, M. A. Siegler, F. Robles, V. M. Chapela, G. Soriano-Moro, E. Pérez-Gutiérrez, J. Bonilla-Cruz and S. Thamotharan, *Cryst. Growth Des.*, 2017, **17**, 1679–1694.

65 M. J. Percino, M. Cerón, O. Rodríguez, G. Soriano-Moro, M. E. Castro, V. M. Chapela, M. A. Siegler and E. Pérez-Gutiérrez, *Molecules*, 2016, **21**, 389.

66 P. Venkatesan, M. Cerón, S. Thamotharan, F. Robles and M. J. Percino, *CrystEngComm*, 2018, **20**, 2681–2697.

67 P. Venkatesan, S. Thamotharan, A. Ilangovan, H. Liang and T. Sundius, *Spectrochim. Acta, Part A*, 2016, **153**, 625–636.

68 P. Venkatesan, V. Rajakannan, N. S. Venkataramanan, A. Ilangovan, T. Sundius and S. Thamotharan, *J. Mol. Struct.*, 2016, **1119**, 259–268.

69 M. Udayakumar, J. Kothandapani, S. S. Ganesan, N. S. Venkataramanan, S. Madan Kumar, K. Byrappa and S. Thamotharan, *J. Mol. Struct.*, 2017, **1133**, 510–518.

70 J. Tomasi, B. Mennucci and R. Cammi, *Chem. Rev.*, 2005, **105**, 2999–3094.

71 S. Miertuš, E. Scrocco and J. Tomasi, *Chem. Phys.*, 1981, **55**, 117–129.

72 W. Kohn and L. J. Sham, *Phys. Rev.*, 1965, **140**, A1133–A1138.

73 A. D. Bochevarov, E. Harder, T. F. Hughes, J. R. Greenwood, D. A. Braden, D. M. Philipp, D. Rinaldo, M. D. Halls, J. Zhang and R. A. Friesner, *Int. J. Quantum Chem.*, 2013, **113**, 2110–2142.

74 J. Breu, P. Stössel, S. Schrader, A. Starukhin, W. J. Finkenzeller and H. Yersin, *Chem. Mater.*, 2005, **17**, 1745–1752.

75 A. D. Becke, *J. Chem. Phys.*, 1993, **98**, 5648–5652.

76 C. Lee, W. Yang and R. G. Parr, *Phys. Rev. B: Condens. Matter Mater. Phys.*, 1988, **37**, 785–789.

77 B. Miehlich, A. Savin, H. Stoll and H. Preuss, *Chem. Phys. Lett.*, 1989, **157**, 200–206.

78 X. Chen, C. Jia, Z. Wan, J. Feng and X. Yao, *Org. Electron.*, 2014, **15**, 2240–2249.